Electrochemical, ^{6}Li MAS NMR, and X-ray and Neutron Diffraction Study of $LiCo_xFe_yMn_{2-(x+y)}O_4$ Spinel Oxides for High-Voltage Cathode Materials

R. Alcántara,* M. Jaraba, P. Lavela, and J. L. Tirado

Laboratorio de Química Inorgánica, Universidad de Córdoba, Edificio C3, planta 1, Campus de Rabanales, 14071 Córdoba, Spain

Received July 17, 2002. Revised Manuscript Received January 6, 2003

$LiCo_xFe_yMn_{2-(x+y)}O_4$ compounds (with $x = 0.2$, 0.4, 0.8, and 1, and $y = 0.0$, 0.2, and 0.4) have been prepared. Substitution of manganese by iron and/or cobalt decreases the cubic lattice parameter. The structure of $LiCo_{0.2}Fe_{0.2}Mn_{1.6}O_4$ has been studied in detail by Rietveld refinement of the structure by using data obtained from neutron diffraction measurements. The electrochemical behavior has been tested in $Li|LiPF_6(EC:DEC)|LiCo_xFe_yMn_{2-(x+y)}O_4$ cells, where an increase of the extension of the capacity delivered in the 5-V region and a decrease for the 4-V region was observed when manganese was substituted by iron and/or cobalt. The changes observed in the X-ray diffraction patterns upon lithium extraction have been studied for $LiCoMnO_4$, $LiCo_{0.8}Fe_{0.2}MnO_4$, and $LiCo_{0.2}Fe_{0.2}Mn_{1.6}O_4$. For all these samples a single cubic phase in which the lattice parameter decreases with lithium extraction was observed. The lattice contraction is more marked for $Li_{1-z}Co_{0.2}Fe_{0.2}Mn_{1.6}O_4$ (from 8.187(1) Å to ca. 8.06 Å) and occurs mostly in the region near 4 V. The novel compound $LiCo_{0.8}Fe_{0.2}MnO_4$ is shown to be a good 5-V cathode material with an initial discharge capacity of 100 $mAhg^{-1}$.

Introduction

During the past decade, the $LiMn_2O_4$ phase with a spinel-related structure has been evaluated as an alternative cathode material to the successful $Li_xC_6/LiCoO_2$ lithium-ion battery.[1,2] Unfortunately, the problems associated with capacity fade have hindered an extended application of this solid. To improve the 3-V and 4-V cycling performances of $LiMn_2O_4$ several cation-substituted phases have also been studied in detail.[3−5] More recently, several spinel-type compounds with general formula $LiM_xMn_{2-x}O_4$ (M = Fe, Ni, Co, Cu, etc.) have been proposed as cathode materials that use a high-voltage capacity around 5 V.[4−7] In these materials the operation voltage changes with the nature of M and the value of x. The possible combination of 5-V electrodes with negative electrodes that work significantly above 0 V, such as titanium oxides,[8] could benefit from the absence of lithium metal deposition, a problem commonly found in the graphite-based electrodes of the "conventional" lithium-ion battery. Some problems of this new concept of lithium-ion battery are the suppression of the 4-V region of the cathode, and the electrolyte decomposition by reaction with the cathode at high voltage. The electrochemical process taking place at about 5 V involves changes in the oxidation state of the transition metal M, rather than the Mn^{4+}/Mn^{3+} pair which takes place about 4 V. In the case of the nickel−manganese spinel $LiNi_{0.5}Mn_{1.5}O_4$, the plateau at ca. 4.8 V is caused by Ni^{2+} to Ni^{4+} oxidation.[5−7,9] However, deviations from the $LiNi_{0.5}Mn_{1.5}O_4$ stoichiometry are commonly found in the preparation of this solid and $Li_xNi_{1-x}O$ impurities have been identified[9] that decrease the 5-V gravimetric capacity. Moreover, the resulting Ni-deficiency in the spinel phase involves the presence of Mn^{3+} which leads to a significant extension of the 4-V plateau at the expense of the nominal 142 $mAhg^{-1}$ 5-V capacity.

On the other hand, the mechanism of the electrochemical reactions of $Li_xMn_2O_4$ in the 4-V region has been the subject of extensive work. In 1996, Xia and Yoshio[10] proposed a one-phase model during lithium insertion extraction at this voltage range. Later, Yang et al.[11] showed in-situ synchrotron X-ray diffraction evidence of the occurrence of three different cubic phases and two regions of two-phase coexistence in the $0 < x < 1$ composition range. These authors also showed that increasing the charge−discharge rate could result in apparent changes in the intermediate phases detected

* To whom correspondence should be addressed. Phone: +34 957 218637. E-mail: iq2alror@uco.es.

(1) Flandrois, S.; Simon, B. *Carbon* **1999**, *37*, 165.
(2) Winter, M.; Besenhard, J. O.; Spahr, M. E.; Novak, P. *Adv. Mater.* **1998**, *10*, 725.
(3) Xia, Y.; Sakai, T.; Fujieda, T.; Wada, M.; Yoshinga, H. *Electrochem. Solid State Lett.* **2001**, *4*, A9.
(4) Ein-Eli, Y.; Howard, W. F., Jr.; Lu, S. H.; Mukerjee, S.; McBeen, J.; Vaughey, J. T.; Thackeray, M. M. *J. Electrochem. Soc.* **1998**, *145*, 1238.
(5) Kawai, H.; Nagata, M.; Tukamoto, H.; West, A. R. *J. Power Sources* **1999**, *81−82*, 67.
(6) Ohzuku, T.; Takeda, S.; Iwanaga, M. *J. Power Sources* **1999**, *81−82*, 90.
(7) Kawai, H.; Nagata, M.; Kageyama, H.; Tukamoto, H.; West, A. R. *Electrochim. Acta* **1999**, *45*, 315.
(8) Scrosati, B.; Panero, S.; Reale, P.; Satolli, D.; Aihara, Y. *J. Power Sources* **2002**, *105*, 59.
(9) Zhong, Q.; Bonakdarpour, A.; Zhang, M.; Gao, Y.; Dahn, J. R. *J. Electrochem. Soc.* **1997**, *144*, 205.
(10) Xia, Y.; Yoshio, M.; *J. Electrochem. Soc.* **1996**, *143*, 825.
(11) Yang, X. Q.; Sun, X.; Lee, S. J.; McBreen, J.; Mukerjee, S.; Daroux, M. L.; Xing, X. K. *Electrochem. Solid-State Lett.* **1999**, *2*, 157.

10.1021/cm021263q CCC: $25.00
Published on Web 02/14/2003

by diffraction procedures. More recently, Xia et al.[12] have shown the role of oxygen deficiency on the detection of the two phase regions. The formation of two cubic phases during the lithium extraction of $LiNi_{0.5}Mn_{1.5}O_4$ has been recently reported.[13]

Concerning iron-containing spinels, the discovery of the high-voltage plateau centered at 4.9 V found by Kawai et al.[14] for $Li_2FeMn_3O_8$ allowed these authors to suggest its possible applications as a cathode material in high-voltage Li-ion batteries. In comparison with $Li_2CoMn_3O_8$, they also highlighted the potential economical and environmental advantages. However, further work to improve the capacity and cycling performance of the plateau centered at 4.9 V was found to be needed. A complete study of different $LiFe_yMn_{2-y}O_4$ compositions was recently carried out by Ohzuku et al.[15] Moreover, the double Co−Fe doping has shown to have a positive effect on the cycling life of $LiM_xMn_{2-x}O_4$ (M = Fe−Co) spinel-type cathode materials,[16] and the $Li_4Ti_5O_{12}/LiCo_{0.2}Fe_{0.2}Mn_{1.6}O_4$ lithium-ion cell has been described.[17]

In this work, $LiCo_xFe_yMn_{2-(x+y)}O_4$ compounds (with x = 0.2, 0.4, 0.8, and 1, and y= 0.0, 0.2, and 0.4) are obtained, and the structure changes and the electrochemical performance when they are used as high-voltage electrodes are evaluated. The mechanism of electrochemical lithium extraction reaction is studied in order to gain a better understanding of the parameters involved in the changes of electrochemical performance.

Experimental Section

Preparation of the $LiCo_xFe_yMn_{2-(x+y)}O_4$ compounds was carried out by a lithium-excess solid-precursor method described elsewhere,[13] using manganese acetate, cobalt nitrate, and iron oxalate as starting compounds. The obtained solid precursor was powdered and annealed at 400 °C under an air atmosphere. The low-crystallinity product was re-ground in an agate mortar and reannealed at 800 °C, during 1 day in the case of the iron-free samples, and during 3 days in the case of iron- and cobalt-containing samples, in an air atmosphere, and slowly cooled to room temperature. The chemical composition of the obtained products was checked by atomic absorption spectroscopy (AAS).

X-ray powder diffraction (XRD) patterns were recorded on a Siemens D5000 instrument, using Cu Kα radiation, and equipped with a graphite monochromator. The electrodes for ex-situ XRD were prepared inside the glovebox by opening the electrochemical cells, placing the products on a glass sample-holder, and covering them with a plastic film to avoid exposure to air.

Neutron diffraction experiments were carried out on the high-resolution D1A diffractometer of the Institute Laue-Langevin (ILL, Grenoble, France) with wavelength 1.91140 Å, step 0.050° (2θ), and data acquisition time of 4 h by each sample. The results were refined with the *Fullprof* program.

^{6}Li nuclear magnetic resonance (NMR) spectra were registered at room temperature in a Bruker ACP400 instrument, taking as reference a 1 M aqueous solution of LiCl, at 58.86 MHz of resonance frequency and a spinning rate of 5.5 kHz.

The electrochemical behavior was tested by using two-electrode Swagelok cells of the type Li|$LiPF_6$(EC:DEC)|$LiCo_xFe_yMn_{2-(x+y)}O_4$. The positive electrodes, having 2.6−9.5 mg cm^{-2} of active material supported on an aluminum foil, were prepared as 9-mm-diameter disks by drying at 120 °C under vacuum for 2 h and pressing a mixture of 86% of the active oxide, 6% of PVDF binder, and 8% of carbon. Lithium electrodes consisted of a clean 9-mm-diameter lithium metal disk. The commercial electrolyte solution (Merck LP40: 1 M $LiPF_6$ in a 1:1 w/w mixture of ethylene carbonate (EC) and diethyl carbonate (DEC)) was supported by porous glass-paper disks from Whatman. The electrochemical curves were carried out using a multichannel MacPile II system. Galvanostatic cycling experiments were performed at C/20 rate (i.e., one Li extracted from $LiCo_xFe_yMn_{2-(x+y)}O_4$ in 20 h) or, alternatively, at C/5.

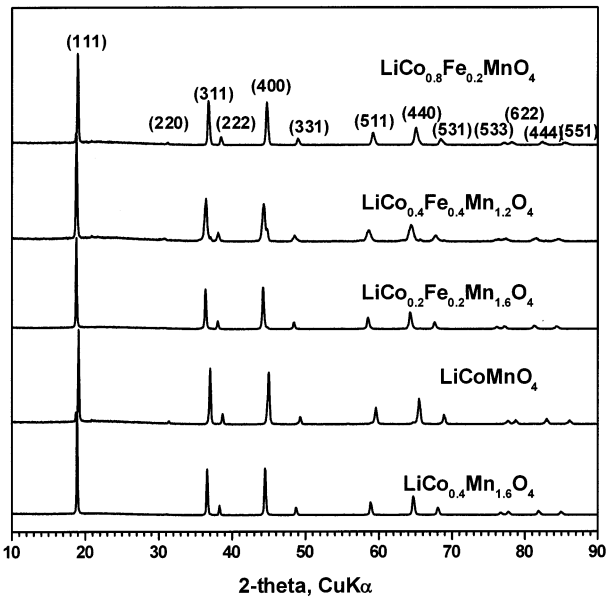

Figure 1. X-ray diffraction patterns of selected $LiCo_xFe_yMn_{2-(x+y)}O_4$ samples obtained at 800 °C. Miller indexes are indicated.

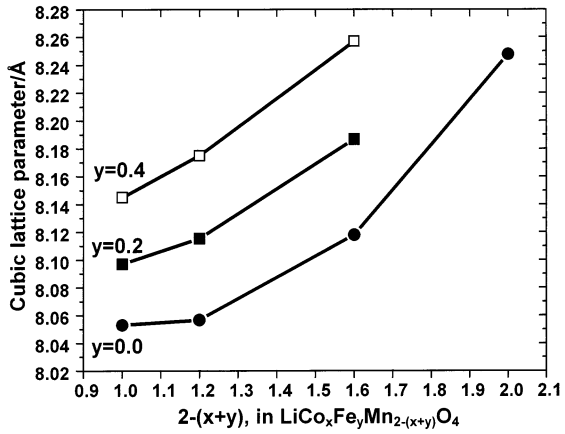

Figure 2. Evolution of cubic lattice parameter in $LiCo_xFe_yMn_{2-(x+y)}O_4$ samples as a function of manganese substitution for iron content (y) equal to: 0.0 (●), 0.2 (■), and 0.4 (□). Data for $LiMn_2O_4$ and $LiFe_{0.4}Mn_{1.6}O_4$ were taken from JCPDS file and ref 15, respectively.

Results and Discussion

The XRD patterns of selected $LiCo_xFe_yMn_{2-(x+y)}O_4$ samples are shown in Figure 1. For y < 0.4, high-purity spinel products were observed and the patterns could

(12) Xia, Y.; Sakai., T.; Fujieda, T.; Yasng, X. Q.; Sun, X.; Ma, Z. F.; McBreen, J.; Yoshio, M. *J. Electochem. Soc.* **2001**, *148*, A723.
(13) Alcántara, R.; Jaraba, M.; Lavela, P.; Tirado, J. L. *Electrochim. Acta* **2002**, *47*, 1829.
(14) Kawai, H.; Nagata, M.; Tabuchi, M.; Tukamoto, H.; West, A. R. *Chem. Mater.* **1998**, *10*, 3266.
(15) Ohzuku, T.; Ariyoshi, K.; Takeda, S.; Sakai, Y. *Electrochim. Acta* **2001**, *46*, 2327.
(16) Bonino, F.; Panero, S.; Satolli, D.; Scrosati, B. *J. Power Sources* **2001**, *97*−*98*, 389.
(17) Panero, S.; Satolli, D.; Salomon, M.; Scrosati, B. *Electrochem. Commun.* **2000**, *2*, 810.

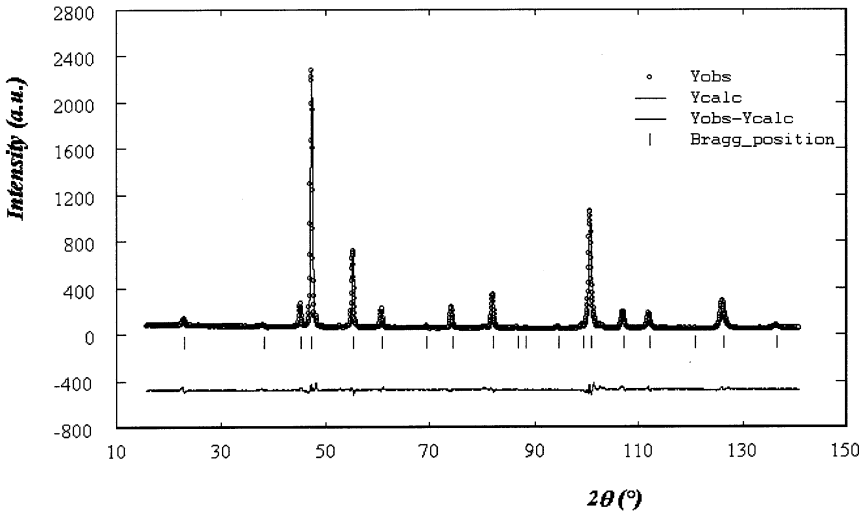

Figure 3. Experimental neutron diffraction pattern and Rietveld refinement of sample $LiCo_{0.2}Fe_{0.2}Mn_{1.6}O_4$.

Table 1. Rietveld Refinements Results of the Neutron Diffraction Pattern of $LiCo_{0.2}Fe_{0.2}Mn_{1.6}O_4$ ($Fd\bar{3}m$ Space Group and $z = 8$)[a]

formula	cell parameter	atom	site	x	y	z	site occupancy	*B* iso.
$LiCo_{0.2}Fe_{0.2}Mn_{1.6}O_4$	8.2258 Å	Li	8a	0.125	0.125	0.125	1.0	2.35
		Mn	16d	0.5	0.5	0.5	1.6	0.09
		Fe	16d	0.5	0.5	0.5	0.2	0.09
		Co	16d	0.5	0.5	0.5	0.2	0.09
		O	32e	0.263	0.263	0.263	4	1.55

[a] $R_{Bragg} = 2.73$. $R_p = 5.54$. $R_{wp} = 7.89$. $R_{exp} = 3.47$.

be indexed in a single cubic lattice with typical reflection conditions of the $Fd\bar{3}m$ space group. For high cation doping levels ($x + y > 0.4$) the presence of Li_2MnO_3 and M_3O_4 impurities was detected. From the unit cell parameter of the impurity phase it was possible to discern Fe_3O_4 as the main side product. On the other hand, the intensity of the (220) line was low or remained undetectable in some samples (Figure 1), suggesting that only lithium ions are located in the tetrahedral 8a sites. However, this result is evaluated below in the light of neutron diffraction data.

Figure 2 shows the cubic unit cell parameters corresponding to the main phase in each sample. Substitution of manganese by cobalt or iron/cobalt tends to decrease the cubic cell parameter. The observed decrease in the unit cell dimensions with cobalt addition agrees with earlier reported data[7,18,19] and matches the lower ionic size of low-spin Co^{3+} (0.545 Å) as compared with high-spin Mn^{3+} (0.645 Å).[20] In contrast, different authors[14,15] have shown that the addition of iron exclusively results in a slight increase in the unit cell parameter. For a sample with nominal composition $LiCo_{0.2}Fe_{0.2}Mn_{1.6}O_4$, in which Fe and Co are included simultaneously, Scrosati et al.[8] observed a value of 8.210 Å, which is lower than the 8.245 Å for the $LiMn_2O_4$ spinel.[21] In our samples, a similar net decrease is observed for all the studied compositions, which provides evidence that the contracting effect of low-spin Co^{3+} prevails to the opposite effect of iron substitution. Moreover, for constant manganese substitution ($x + y$ value) on increasing iron substitution (y value) an increase in the lattice parameter is observed (Figure 2). This is again consistent with the higher ionic radius of high-spin Fe^{3+}(0.645 Å) as compared with that of low-spin Co^{3+}(0.545 Å).

A better knowledge of the cation distribution into the spinel sites was achieved by Rietveld refinement of neutron diffraction patterns of $LiCo_{0.2}Fe_{0.2}Mn_{1.6}O_4$. The experimental diffraction pattern shown in Figure 3 was studied by using a single-phase model with the results shown in Table 1. Attempts to allow a partial occupancy of tetrahedral 8a sites by iron resulted in a poor fit. The best R_{BRAGG} of 2.73 was obtained when 8a site occupancy was restricted to lithium ions. Similarly, the refinement demonstrated the complete occupancy of 16d sites by cobalt, iron, and manganese ions in the stoichiometric ratio. These results agree well with the previous report by Ohzuku et al., in which all iron ions were shown to be located at the 16d sites when $0 < y < 0.6$ in $LiFe_yMn_{2-y}O_4$.[15]

Figure 4 shows the ^6Li MAS NMR spectra of selected samples, in which the unpaired electrons clearly perturb the observed signals. In contrast with manganese substitution in $LiM_xMn_{2-x}O_4$ by Li, Zn, Ni, Cr, and Al, replacement by Co decreases the magnetic susceptibility of the spinel.[22] This is correlated with the different spectra of $LiCoMnO_4$ and $LiCo_{0.4}Mn_{1.6}O_4$ obtained here. The main signal corresponding of $LiCoMnO_4$ is located at ca. 400 ppm (Figure 4a), which can be ascribed to lithium in tetrahedral sites, and less intense peaks of lithium in close proximity to lattice defects (i.e., manganese vacancy, or manganese substitution) are also

(18) Guohua, L.; Ikuta, H.; Uchida, T.; Wakihara, M. *J. Electrochem. Soc.* **1996**, *143*, 178.
(19) Zhecheva, E.; Stoyanova, R.; Gorova, M.; Lavela, P.; Tirado, J. L. *Solid State Ionics* **2001**, *140*, 19.
(20) Shannon, R. D. *Acta Crystallogr.* **1976**, A *23*, 751.
(21) Thackeray, M. M. *Prog. Solid State Chem.* **1997**, *25*, 1.
(22) Tucker, M. C.; Reimer, J. A.; Cairns, E. J. *J. Electrochem. Soc.* **2001**, *148*, A951.

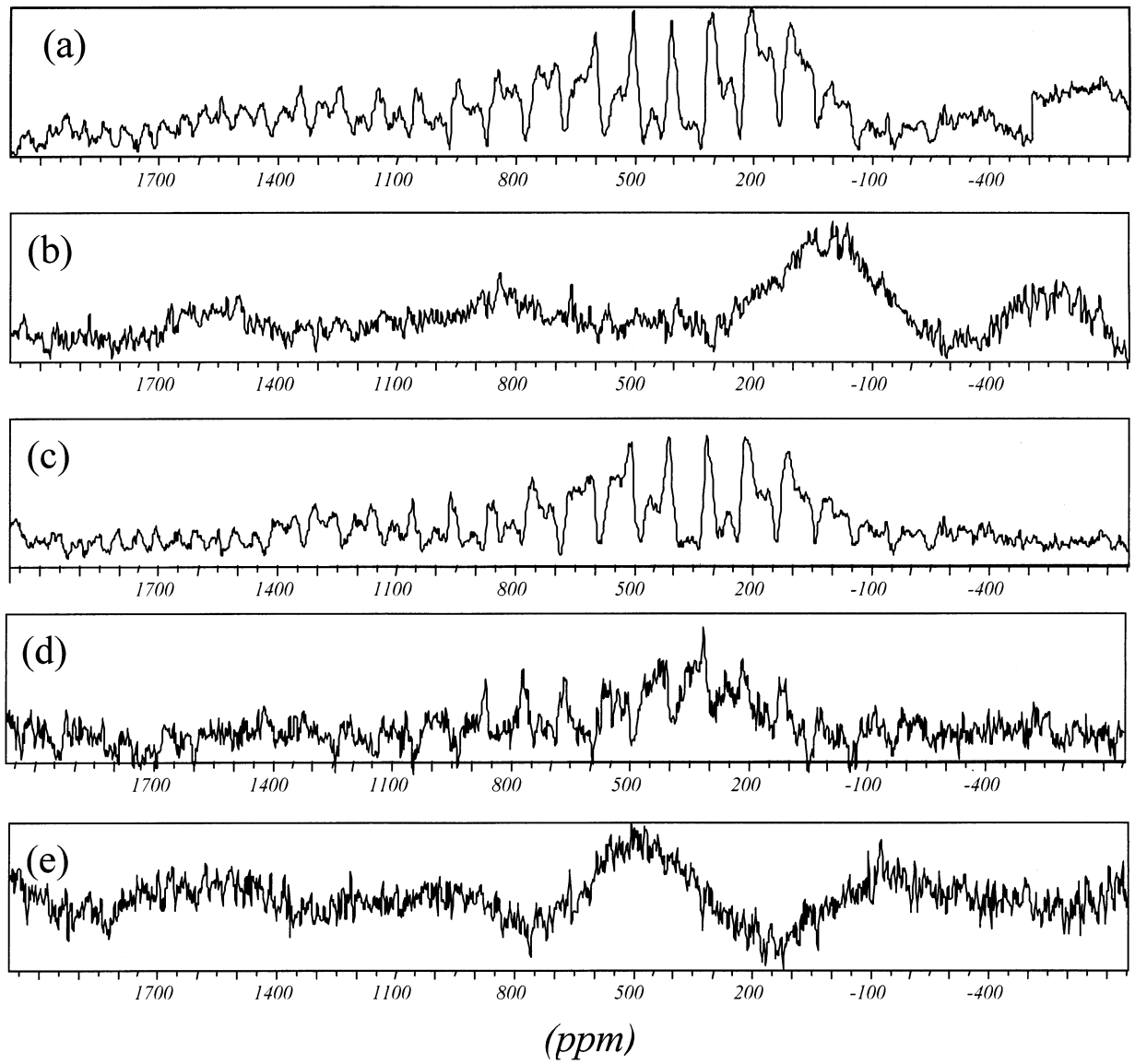

Figure 4. ^{6}Li MAS NMR spectra of (a) $LiCoMnO_4$, (b) $LiCo_{0.4}Mn_{1.6}O_4$, (c) $LiCo_{0.8}Fe_{0.2}MnO_4$, (d) $LiCo_{0.6}Fe_{0.2}Mn_{1.2}O_4$, and (e) $LiCo_{0.2}Fe_{0.2}Mn_{1.6}O_4$.

present.[22,23] Rotational sidebands, assignable by recording the spectra at different spin rates, are also observed. However, in the case of $LiCo_{0.4}Mn_{1.6}O_4$ (Figure 4b) very broad bands are observed. For the simultaneous substitution by iron and cobalt, the differences between $LiCo_{0.8}Fe_{0.2}MnO_4$ (Figure 4c) and $LiCo_{0.2}Fe_{0.2}Mn_{1.6}O_4$ (Figure 4e) are equivalent to those previously discussed for $LiCoMnO_4$ and $LiCo_{0.4}Mn_{1.6}O_4$. Finally, $LiCo_{0.6}Fe_{0.2}Mn_{1.2}O_4$ (Figure 4d) shows an intermediate behavior. Summarizing, two different types of spectra are observed for $LiCo_xFe_yMn_{2-(x+y)}O_4$ compounds: for $x + y$ approaching unity, several resolved signals are observed between 200 and 500 ppm. For $x + y$ significantly lower than unity, broadened resonances at 540 and 800−900 ppm occur. According to different studies on the application of NMR techniques to $LiMn_2O_4$-related solids,[23−27] the shift to higher frequency is consistent with increasing manganese oxidation state. Thus, the ^{6}Li NMR resonances of Li cations in lithium manganese oxides shift from 36−143 ppm for Mn^{3+} ions to 500 ppm for the mixed-valent Mn^{3+}/Mn^{4+} compounds, and to 700−850 ppm for Mn^{4+}. Moreover, for Ni-doping, at least four resonances are observed at 503, 567, 638, and 690 ppm.[25] All these observations agree with our experiments.

Some of the spectra in Figure 4 contain weak signals in the 1500−2000 ppm range. Signals with chemical shifts close to 2000 ppm have been assigned in recent papers to the presence of lithium in 16d octahedral sites either by the occurrence of a lithium excess in the $Li_{1+x}Mn_{2-x}O_4$ series,[22,27] or by manganese substitution by cations with a strong preference for tetrahedral sites, which results in lithium migration to the octahedral sites, as occurs in the $LiZn_xMn_{2-x}O_4$ series.[26] However, the X-ray patterns denote a smaller intensity of the (220) reflection than expected for transition metal atoms

(23) Lee, Y. J.; Wang, F.; Grey, C. P. *J. Am. Chem. Soc.* **1998**, *120*, 12601.
(24) Lee, Y. J.; Grey, C. P. *Chem. Mater.* **2000**, *12*, 3871.
(25) Lee, Y. J.; Eng, C.; Grey, C. P. *J. Electrochem. Soc.* **2001**, *148*, A249.
(26) Lee, Y. J.; Park, S.-H.; Eng, C.; Parise, J. B.;. Grey, C. P *Chem. Mater.* **2002**, *14*, 194.
(27) Lee, Y. J.; Grey, C. P.; *J. Electrochem. Soc.* **2002**, *149*, A103.

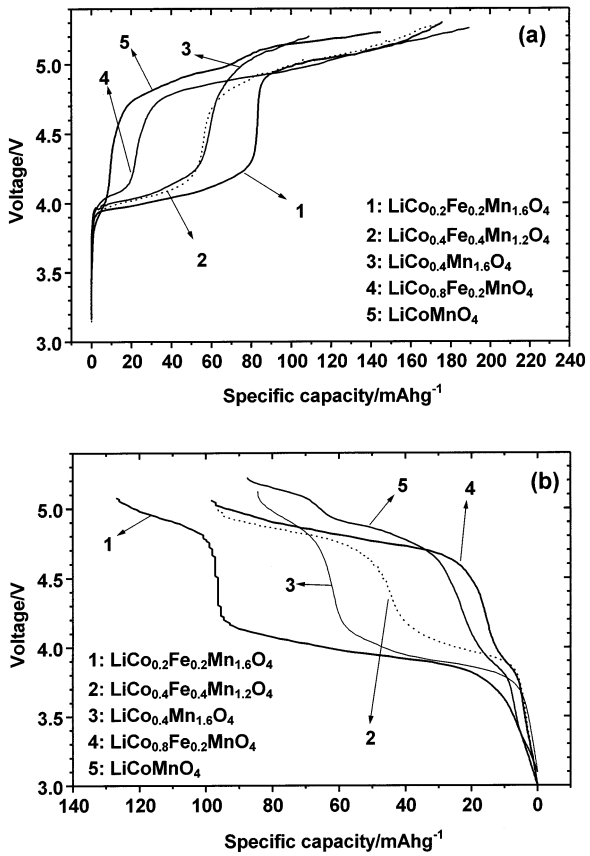

Figure 5. Typical voltage vs capacity curves corresponding to (a) charge and (b) discharge of selected $LiCo_xFe_yMn_{2-(x+y)}O_4$ samples in lithium cells. Rate: C/20.

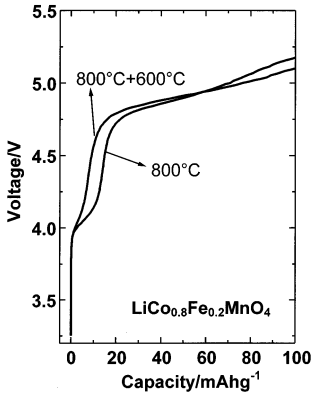

Figure 6. Comparison of voltage vs capacity curves in the first charge of Li|$LiPF_6$(EC:DEC)| $LiCo_{0.8}Fe_{0.2}MnO_4$ cells for cathode material obtained at 800 °C and postannealed at 600 °C. Rate: C/5.

in the 8a tetrahedral sites. Moreover, Rietveld refinement of the structure of slowly cooled $LiCo_{0.2}Fe_{0.2}Mn_{1.6}O_4$ does not require the inclusion of Li in 16d sites in order to obtain a good fit. Thus, one can conclude that octahedral Li is not present in our spinel samples. In consequence, the signals in the 1500−2000 ppm range observed in the spectra can be ascribed to Li_2MnO_3 impurities, often found at high cation-doping levels, as described by Lee et al.[26]

Figures 5−7 show the electrochemical results of Li|$LiPF_6$(EC:DEC)|$LiCo_xFe_yMn_{2-(x+y)}O_4$ cells under galvanostatic conditions. The first charge and discharge branches are compared for several sample compositions in Figure 5a and b, respectively. The incorporation of

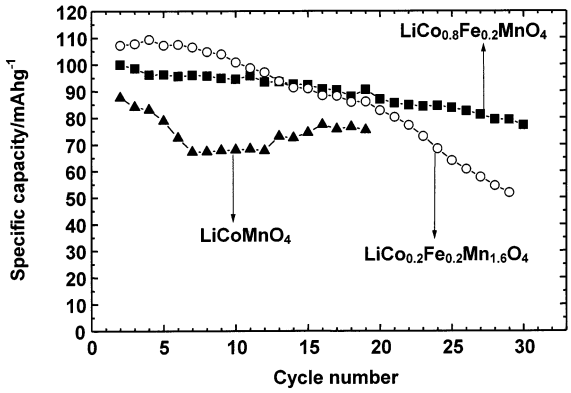

Figure 7. Capacity evolution on cycling of Li|$LiPF_6$(EC:DEC)|$LiCo_xFe_yMn_{2-(x+y)}O_4$ cells. Rate: C/20.

iron and cobalt in the manganese spinel changes the shape of the voltage vs capacity curves in both the branches. For a manganese substitution lower than one manganese per formula ($x + y < 1$) an extended pseudo-plateau at ca. 4 V is observed, which corresponds to the oxidation from Mn^{3+} to Mn^{4+}. It should be noted that even in those samples in which the expected oxidation state of manganese is 4+, i.e., for $x + y = 1$, a short 4-V region is still observed. However, the 4-V region decreases in extension by reannealing the samples at 600 °C under an air atmosphere (Figure 6). In addition, all samples show a pseudo-plateau of different extension at about 5 V. According to the literature for iron-containing samples, ^{57}Fe Mössbauer spectroscopy unambiguously shows that Fe^{3+} to Fe^{4+} oxidation takes place around 4.9 V.[14,17] Also, the voltage of Co^{3+} to Co^{4+} oxidation is close to this value.[5,6] The monophasic nature of both electrochemical processes discussed below agrees well with the nonzero slope of the curves in these regions, characteristic of a solid solution intercalation host model.

A maximum reversible capacity of ca. 130 $mAhg^{-1}$ is achieved for $LiCo_{0.2}Fe_{0.2}Mn_{1.6}O_4$ in the complete potential range, including 4- and 5-V pseudo-plateaus. However, the progressive substitution of manganese (up to $x + y = 1$) results in a reduction of the 4-V region and an increase of the extension of a 5-V pseudo-plateau. Simultaneously, the total reversible capacity decreases, and the changes are more pronounced than those expected exclusively from the higher atomic weights of the substituents. In fact, for $x + y = 1$, the charge process must be completed well above 5.1 V, and, henceforth, irreversible electrolyte decomposition is produced in unknown extension. Thus, charge capacity in Figure 5a is not directly equivalent to the amount of extracted lithium. Nevertheless, the experimental maximum capacity value (100 $mAhg^{-1}$) for simultaneous cobalt and iron substitution of one manganese per formula is comparable to that previously reported for $LiCoMnO_4$.[7]

The experimental total discharge capacity upon cycling for selected samples is shown in Figure 7. Considering the effect of electrolyte decomposition in the extended 5-V pseudo-plateau at C/20 rate, the capacity and capacity retention at 5 V are promising for $LiCo_{0.8}Fe_{0.2}MnO_4$. For $LiCo_{0.2}Fe_{0.2}Mn_{1.6}O_4$ the initial total capacity is the highest (109 $mAhg^{-1}$), but it includes both the 4-V and the 5-V regions. Capacity fading is

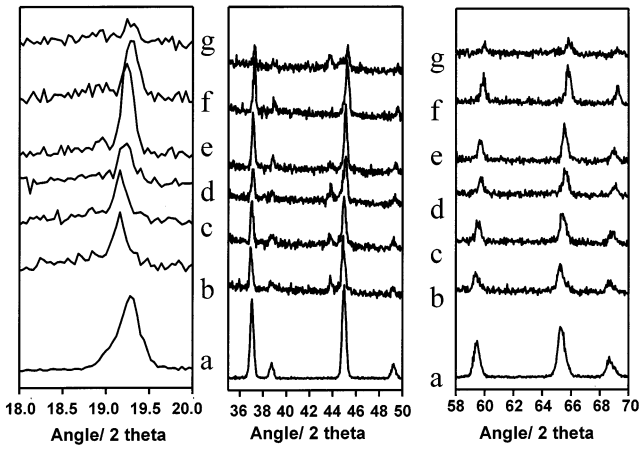

Figure 8. Ex-situ X-ray diffraction patterns of (a) raw $LiCo_{0.8}Fe_{0.2}MnO_4$, and corresponding electrodes after (b) 35 $mAhg^{-1}$, (c) 60 $mAhg^{-1}$, (d) 93 $mAhg^{-1}$, (e) 102 $mAhg^{-1}$, (f) 131 $mAhg^{-1}$, and (g) 153 $mAhg^{-1}$ of the first charge.

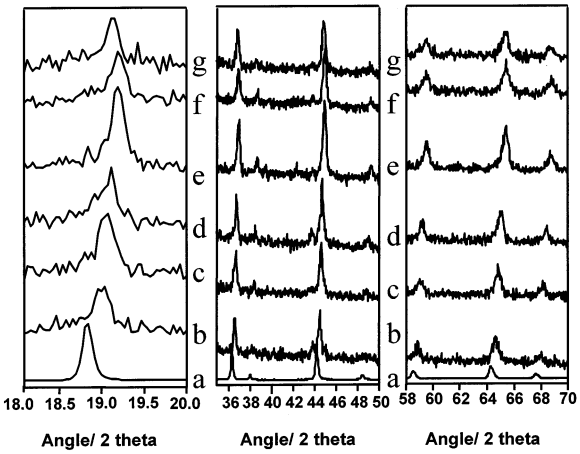

Figure 9. Ex-situ X-ray diffraction patterns of (a) raw $Li_zCo_{0.2}Fe_{0.2}Mn_{1.6}O_4$, and corresponding electrodes after (b) 21 $mAhg^{-1}$, (c) 30$mAhg^{-1}$, (d) 45 $mAhg^{-1}$, (e) 100 $mAhg^{-1}$, (f) 146 $mAhg^{-1}$, and (g) 147 $mAhg^{-1}$ of the first charge.

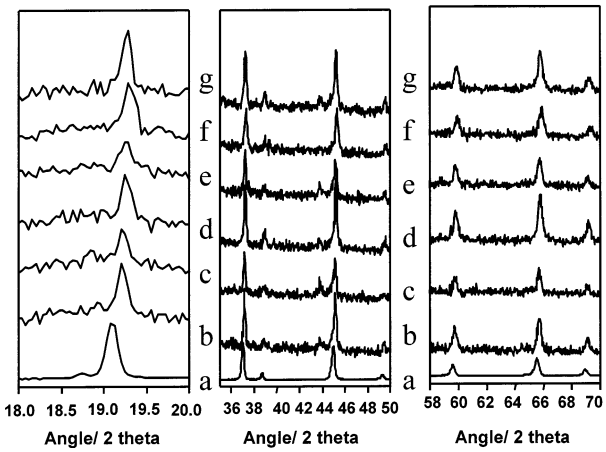

Figure 10. Ex-situ X-ray diffraction patterns of (a) raw $LiCoMnO_4$, and corresponding electrodes after (b) 60 $mAhg^{-1}$, (c) 70 $mAhg^{-1}$, (d) 83 $mAhg^{-1}$, (e) 94 $mAhg^{-1}$, (f) 131 $mAhg^{-1}$, and (g) 142 $mAhg^{-1}$ of the first charge.

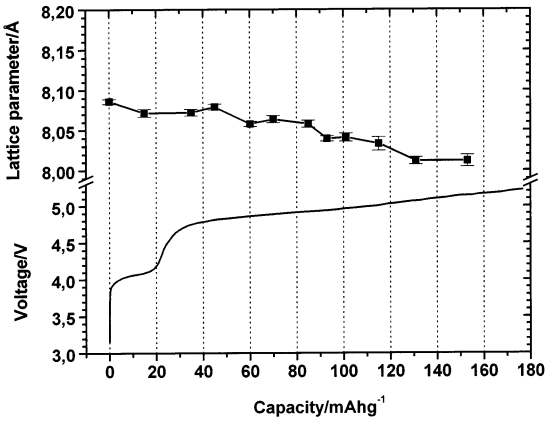

Figure 11. Calculated cubic lattice parameter of $Li_{1-z}Co_{0.8}Fe_{0.2}MnO_4$ electrodes at different depths of the first charge. Voltage vs capacity on charge is shown.

marked for $LiCo_{0.2}Fe_{0.2}Mn_{1.6}O_4$ after 5 cycles. As compared with a similar composition reported by Bonino et al.[16] at C and C/5 rates, the initial discharge capacity in our samples is similar, but capacity retention is poorer on cycling at higher rates. No composition equivalent to $LiCo_{0.8}Fe_{0.2}MnO_4$ with only 5 V contribution was studied by these authors.[16]

Recently, the electrochemical reactions of the pure spinel $Li_xMn_2O_4$ in the 4-V region have been the subject of intensive work and debate. Thus, in 1996, Xia and Yoshio[10] proposed a one-phase model during lithium insertion−extraction at this voltage range. Later, Yang et al.[11] showed by in-situ synchrotron X-ray diffraction evidence of the occurrence of three different cubic phases, and two regions of two-phase coexistence in the $0 < x < 1$ composition range. These authors also showed that increasing the charge−discharge rate could result in apparent changes in the intermediate phases detected by diffraction procedures. More recently, Xia et al.[10] have shown the role of oxygen deficiency on the detection of the two phase regions. The phases emerging by lithium deintercalation from $LiNi_{0.5}Mn_{1.5}O_4$ in the 5-V region were recently identified by our group.[13]

Information on the mechanism of charge reaction in the present materials was also obtained by ex-situ X-ray diffraction recordings (Figures 8−10). Electrochemical experiments were interrupted at selected extensions of charge and the electrode material was examined. The possible surface reactions between electrodes charged up to near 5 V and the electrolyte were minimized by this procedure, as the cells were dismantled immediately after the lithium extraction before the X-ray recordings. Figure 8 shows the selected X-ray diffraction patterns corresponding to $LiFe_{0.2}Co_{0.8}MnO_4$ electrodes at different depths of charge. Contrary to other manganese-containing spinels, a multiphase mechanism with several spinel phases of different lattice parameters is not observed when lithium extraction progresses. However, it should be noted that a new low-intensity line at about 44° 2θ develops on cycling, which could be ascribed to a Li_2MnO_3-related product as found in other works on doped $LiMn_2O_4$.[28,29] Nevertheless, atomic absorption spectroscopy measurements revealed that the Fe/Co and Co/Mn atomic ratios remained basically unchanged during 30 charge−discharge cycles.

Lithium extraction leads to a contraction in the unit cell parameter (Figures 11−13). This contraction is more

(28) Sun, Y. K.; Park, G. S.; Lee, Y. S.; Yoshio, M.; Nahm, K. S. *J. Electrochem. Soc.* **2001**, *148*, A994.
(29) Sun, Y.-K.; Hong, K.-J.; Prakash, J.; Amine, K. *Electrochem. Commun.* **2002**, *4*, 344.

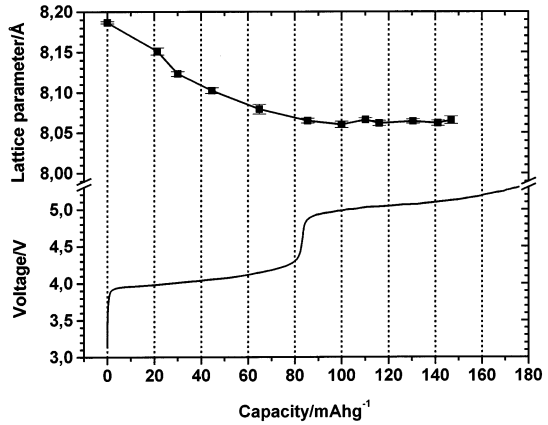

Figure 12. Calculated cubic lattice parameter of $Li_{1-z}Co_{0.2}Fe_{0.2}Mn_{1.6}O_4$ electrodes at different depths of the first charge. Voltage vs capacity on charge is shown.

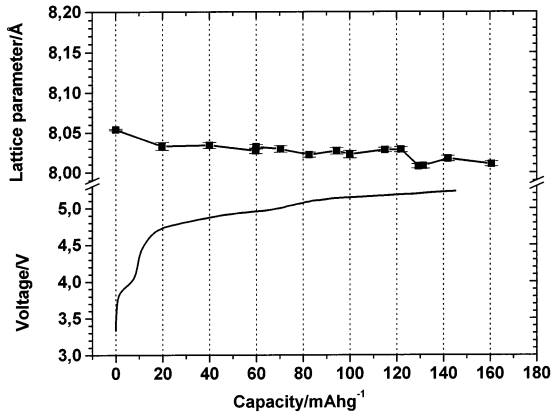

Figure 13. Calculated cubic lattice parameter of $Li_{1-z}CoMnO_4$ electrodes at different depths of the first charge. Voltage vs capacity on charge is shown.

marked in the case of $LiCo_{0.2}Fe_{0.2}Mn_{1.6}O_4$ (from 8.187(1) Å to ca. 8.06 Å, in Figure 12) and it mainly takes place through the 4-V region (about 83 $mAhg^{-1}$ in the voltage vs capacity curve, i.e., 0.6 Li per formula). This behavior can be explained by taking into account the different ionic radii of high−spin Mn^{3+} (0.645 Å) and Mn^{4+} (0.53 Å). After the 4-V region the lattice parameter remains nearly constant. It has been previously reported that the lattice parameter varies from 8.245 Å in $LiMn_2O_4$ to 8.029 Å in Mn_2O_4,[21] which is an even higher variation than that in the $LiCo_{0.2}Fe_{0.2}Mn1.6O_4$ sample studied here. Henceforth, the substitution of manganese by iron and/or cobalt decreases the lattice parameter contraction during the lithium extraction in $LiCo_xFe_yMn_{2-(x+y)}O_4$ samples. Moreover, preservation of pristine structure with a calculated cubic cell parameter (8.069(5) Å) close to that of the non−cycled material (8.086(3) Å) was observed for a $LiCo_{0.8}Fe_{0.2}MnO_4$ electrode after 30 galvanostatic charge/discharge cycles.

Conclusions

A series of $LiCo_xFe_yMn_{2-(x+y)}O_4$ samples have been obtained. Exchange of manganese by iron and/or cobalt, takes place in octahedral sites, and induces significant changes in the cubic lattice cell parameter and the shape of the voltage vs capacity curve in $Li|LiPF_6$(EC:DEC)$|LiCo_xFe_yMn_{2-(x+y)}O_4$ cells. Lithium extraction of $LiCo_xFe_yMn_{2-(x+y)}O_4$ causes lattice contraction in the cubic phase which is less marked when manganese is substituted by iron and/or cobalt. $LiCo_{0.8}Fe_{0.2}MnO_4$, a sample with a composition to our knowledge not previously reported in the literature, exhibits an extended pseudo plateau and an initial 5-V discharge capacity of ca. 100 $mAhg^{-1}$, which remains above 90 $mAhg^{-1}$ during the first 20 cycles.

Acknowledgment. We acknowledge financial support from the European Commission (contract ENK6-CT2000-00082, Negelia) and CICYT (contracts MAT1999-0742 and MAT2000-2721-CE). R.A. is indebted to MCYT (Programa Ramón y Cajal). We also thank the Institute Laue-Langevin, Grenoble, for use of their neutron diffraction facilities.

CM021263Q